Wear 488–489 (2022) 204169

Contents lists available at ScienceDirect

Wear

journal homepage: www.elsevier.com/locate/wear

Precise measurement of worn-out tool diameter using cutting edge features during progressive wear analysis in micro-milling

Suman Saha, Sankha Deb, Partha Pratim Bandyopadhyay *

Department of Mechanical Engineering, Indian Institute of Technology Kharagpur, Kharagpur, West Bengal, 721302, India

ARTICLE INFO

Keywords:
Micro-milling
Edge radius
Tool wear
Tool life
Flank wear

ABSTRACT

Increase in edge radius, decrease in diameter, and growth of flank wear are three commonly used indices for quantitative assessment of the micro-milling tool wear. Worn-out tool diameter is usually measured by observing it under a microscope at low magnification, and this leads to significant measurement error (up to 20% of the tool life). When edge geometry changes with progressive wear, the outer diameter also decreases synchronously. In this article, a correlation between the changes in edge features and the corresponding reduction in outer diameter is developed to calculate the latter more precisely. For this purpose, first, analytical expressions are derived for different wear scenarios (uniform abrasion, non-uniform abrasion, adhesion, and edge-chipping). Validation of these expressions is further carried out through sustainable minimum quantity lubrication (MQL) assisted micro-milling of Ti–6Al–4V using TiAlN-coated WC/6Co micro-mills. Various stages of tool wear are characterized, and suitable parameters for quantifying the same are assessed. While the directly measured diameter values are affected by inconsistency and negative wear rate, the corresponding estimated values vary consistently and reliably with positive wear rate across different regimes. The diameter reduction is further established as the preferred variable for drawing tool life curve in micro-milling.

1. Introduction

Mechanical micro-milling is one tool-based subtractive micro-fabrication process that can produce three-dimensional micro-features on a wide variety of materials requiring minimum effort. Commercial micro-mills are predominantly solid cutters having two flutes with diameter in 100–1000 μm range. As shown in Fig. 1, crucial geometrical features of such micro-tools include rake angle (γ_O), clearance angle (α_O), back clearance angle ($\alpha_O^{'}$), helix angle (ψ), edge radius (r_e), nose radius (r_N), outer diameter (D_C), and number of flutes (Z). The curvature radius at the principal cutting edge where rake surface meets the primary flank surface is termed as edge radius. It is the measure of sharpness of the tool; the lower is the r_e the sharper is the edge. Commercial micro-mills typically have edge radius in between 0.1 and 4.0 μm [1,2]. In micro-milling, the edge radius directly governs the material removal mechanism as chip formation does not initiate until the instantaneous uncut chip thickness exceeds the minimum uncut chip thickness (h_{min}) (Fig. 1c). This h_{min} is proportional to the edge radius with a constant κ ($0.15 \leq \kappa \leq 0.5$) [3].

$$h_{min} = \kappa\, r \tag{1}$$

When a fresh tool is engaged for micro-milling, it inevitably undergoes wear resulting in the changes in edge-geometry and reduction in tool-diameter. Most researchers considered edge radius as the primary index for quantitative assessment of the tool wear in micro-milling. Apart from the edge radius, several authors also measured the changes in tool outer diameter and flank wear length to quantitatively analyse progression of the micro-milling tool wear. Outer diameter of the micro-mill is an equally important factor as it directly influences kerf width and feature accuracy of the milled slot [4].

During micro-milling of Inconel 718 using 768 μm diameter coated carbide cutters, Ucun et al. (2013) [5] reported 6–20% reduction in outer diameter within 120 mm length of cut. During the same duration of machining, edge radius increased to 30–60 μm. Dadgari et al. (2018) [6] also reported 25 μm reduction in diameter after 375 mm micro-milling of Ti–6Al–4V using 1.0 mm uncoated carbide tool. Using TiAlN coated tungsten carbide tools for micro-milling of Ti–6Al–4V, Khaliq et al. (2020) [7] reported 40–50 μm reduction in diameter in dry cutting and 20–30 μm reduction in MQL (minimum quantity lubrication) cutting after 500 mm cut. Within the same length, the edge radius increased to 23–28 μm in dry cutting and 15–18 μm in MQL cutting.

* Corresponding author.
E-mail address: ppb@mech.iitkgp.ac.in (P.P. Bandyopadhyay).

https://doi.org/10.1016/j.wear.2021.204169
Received 24 July 2021; Received in revised form 7 October 2021; Accepted 31 October 2021
Available online 3 November 2021

Sorgato et al. (2020) [8], however, considered the percentage reduction in outer diameter as the only variable to understand the effects of tool wear on the bottom surface quality. Working with 400 μm TiAlN coated carbide tools, Manso et al. (2019) [9] also focused only on the outer diameter reduction to quantitatively express micro-milling tool wear.

As the tool undergoes wear, the quality of micro-milled feature also degrades. The actual machining time up to which a tool renders satisfactory performance is treated as the life of the concerned cutter. Although ISO 8688–2:1989 specifies the standard procedure for tool life testing of macro-scale end-milling cutters, no such standard is available so far for micro-milling tools. As summarized in Table-1, researchers considered various indexes such as outer diameter reduction (ΔD_C), worn-out edge radius ($r_e^{(W)}$), flank wear length (V_B), and average surface roughness (R_a) to draw the micro-milling tool rejection criteria. In one of the early works, De Cristofaro et al. (2012) [10] tested multiple coatings considering 5.8 m length of cut as the tool rejection criteria during dry micro-milling of tool steel using 1.0 mm tungsten carbide cutters. While developing a protocol for progressive tool wear analysis, Alhadeff et al. (2019) [11] suggested considering the rake face wear width of 4% of the tool diameter as tool-life criteria for micro-milling of Ti-alloys. During MQL based micro-milling of titanium alloy using TiAlN-coated tungsten carbide tools, Khaliq et al. (2020) [7] considered either 22 μm flank wear, 28 μm edge radius, or 0.6 μm average roughness as the tool rejection criteria.

Although few studies were carried out focusing on the implementation of the image processing system [15], most researchers by far followed conventional procedure for measuring various features of the worn-out micro-milling tool. In literature, edge radius was commonly measured by observing the bottom-view of the tool under a microscope at high magnification, and thereafter fitting a circle of known diameter at the rounded edge. Flank wear length was also measured by observing the principal cutting edge at a high magnification. On the other hand, measurement of outer diameter of the worn-out tool was commonly performed directly by observing the bottom-view under a microscope at low magnification.

Measurement when carried out at low magnification produces significant measurement error. Given the narrow criteria for the expiry of tool life, this measurement error fetches inaccurate data during tool-wear analysis. For example, when 10% diameter loss is the tool rejection criteria for a 500 μm diameter cutter, a measurement error of ±10 μm can produce 20% error in specifying the tool life. With the short life and expensive nature of the micro-mill, 20% measurement error is usually unacceptable. Several other factors such as non-uniform wear, material adhesion, etc. cannot be distinguished during direct measurement of outer diameter at low magnification. Since the diameter alone cannot portray various types of wear experienced by the cutting edges, Alhadeff et al. (2019) [11] also discouraged the usage of diameter reduction as an index for quantitative assessment of micro-milling tool wear. Even though the edge radius and outer diameter of any micro-mill are two independent features, changes in any one feature lead to a synchronous change in the other one. This article attempts to demonstrate the interrelationship among the changes in edge geometry and reduction in outer diameter so that the diameter reduction can be obtained indirectly but more precisely from the features of the worn-out edges. It may be noted that precise measurement of the outer diameter of the micro-mill is essential for analysis related to feature accuracy, kerf geometry, tool run-out, tool life, etc. Thus, the objectives of this article are as follows.

- To analytically develop the interrelationship between the features of the worn-out cutting edges and the corresponding reduction in outer diameter for various wear scenarios with an aim to retrieve the outer diameter with enhanced accuracy by replacing the conventional direct measurement technique during progressive tool wear analysis.
- To highlight the measurement errors associated with the microscope-based direct measurement technique of the worn-out micro-mill diameter, and the corresponding benefits of the indirect method.
- To distinguish and characterize various stages of tool wear, and the possible ways of quantifying the same using easily measurable parameters during micro-milling of difficult-to-machine material.
- To experimentally demonstrate the procedure for estimating the outer diameter across various wear regimes; and to further explore the feasibility of using outer diameter as the primary index for tool life study with progressive wear of the micro-mill.

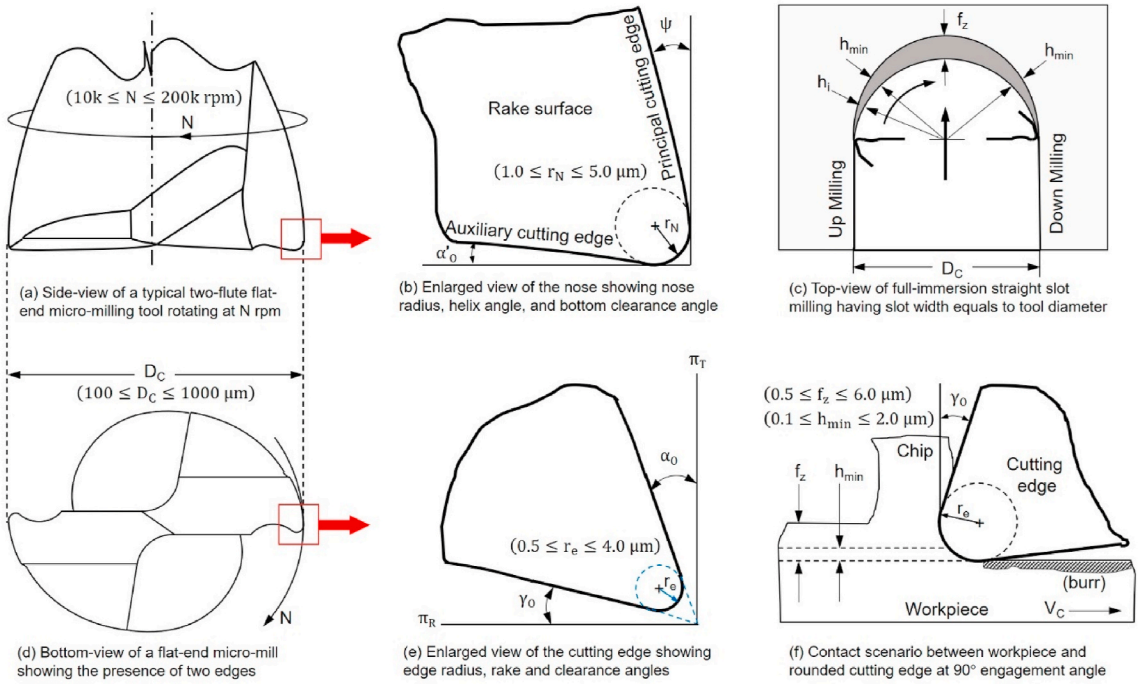

Fig. 1. Schematic representation of crucial geometrical features of the micro end milling tool as well as the tool-workpiece engagement scenario for full-immersion straight slot milling (typical range of various parameters is also provided).

Table-1
Micro-milling tool rejection criteria considered by different researchers.

Ref.	Work material	Tool substrate	Tool coating	Tool diameter (μm)	Tool life expiration criteria			
					ΔD_C (μm)	$r_e^{(W)}$ (μm)	V_B (μm)	R_a (μm)
Lu (2016) [12]	Inconel	WC/6Co	TiAlN	300	66	–	–	–
dos Santos (2018) [13]	SS	Carbide	TiN	381	–	–	12.65	–
Kumar (2019) [14]	Ti64	WC	TiAlN	1000	–	–	15–20	–
Khaliq (2020) [7]	Ti-alloy	WC	TiAlN	500	–	28	22	0.6

In section-2, the relationship between the outer diameter reduction and the worn-out edge geometry is analytically established. Initially, the relationship is demonstrated for the simplest wear scenario where both cutting edges undergo equal degree of wear (initial and final edge radii for both the edges are same). The analysis is further extended for non-uniform abrasion wear and adhesion wear as well. Once the tool experiences chipping, the edge radius cannot be measured appropriately. In such scenario, feasibility of assessing the outer diameter reduction from the flank wear length is analytically demonstrated. Section-3 provides the details of the experimentation and data acquisition during micro-milling of Ti–6Al–4V samples using TiAlN-coated tungsten carbide tools under sustainable minimum quantity lubrication (MQL). In Section-4, various wear regimes are identified, and the estimated outer diameter reduction values are tallied with the directly measured values to emphasis the consistency and reliability of the estimated values. The mechanism of tool wear is also briefly explained in Section-5. Furthermore, the feasibility of drawing the tool-life curve using the outer diameter reduction is explored in Section-6.

2. Analytical development of the relationship between outer diameter reduction and worn-out edge geometry

When a micro-milling tool is engaged for machining a ductile metal, the cutting edges initially undergo abrasive wear leading to an increase in edge radius. With further increase in the length of cut, chip material begins to adhere to the edges. Meanwhile, coating delamination (peeling off) also occurs exposing the substrate material. With further progression of micro-milling, cutting edges undergo edge-chipping leading to complete changes in edge-geometry. The feasibility of estimating outer diameter reduction from the cutting edge geometry of the worn-out tool for the common wear scenarios is explored in the subsequent sections. As the area of interest at the tool-tip is confined to a small portion (10–15 μm), the cutting edge is assumed to have flat rake and flank surfaces within this focused region.

2.1. Uniform abrasion wear of the two-flute micro end mills

Begin with the simplest but most commonly used form of micro end

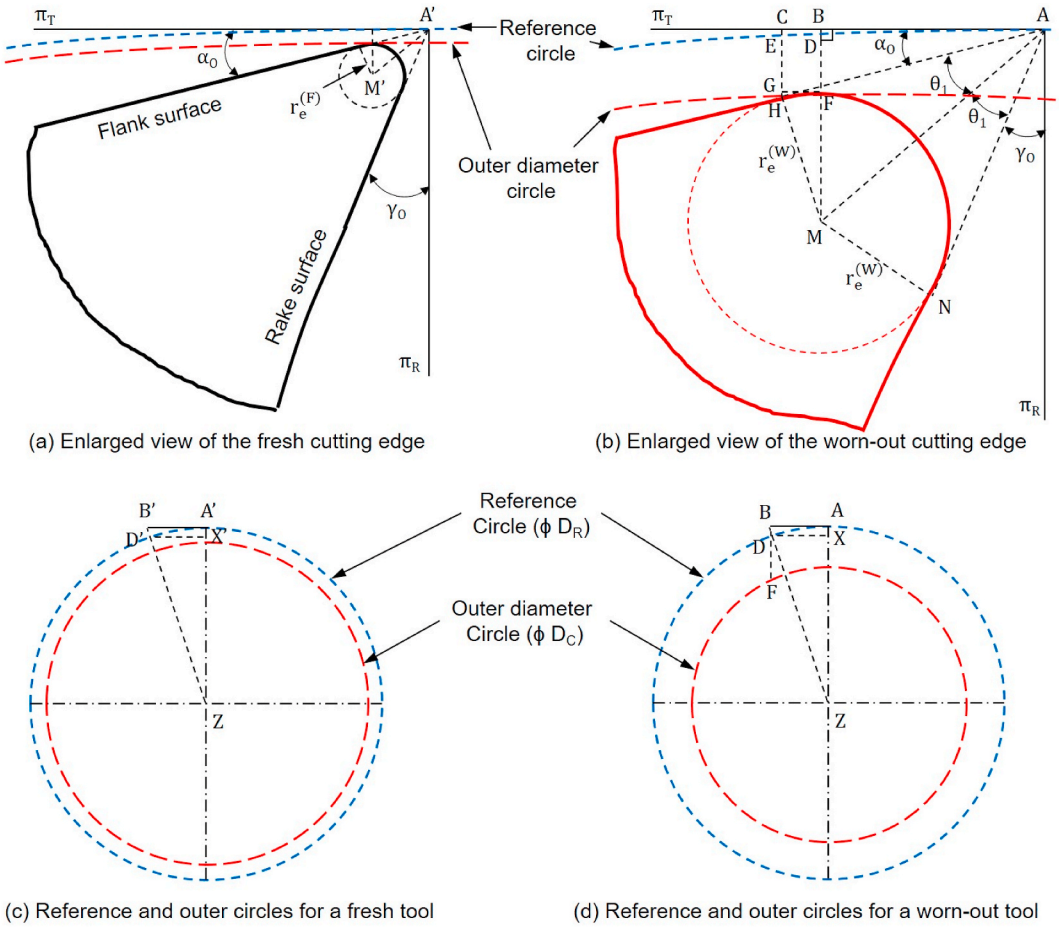

Fig. 2. Schematic representation of the outer diameter reduction scenario owing to uniform increase in the edge radius by abrasion wear.

milling tool having two cutting edges located 180° apart. As schematically shown in Fig. 2a, the fresh tool has a small edge radius of $r_e^{(F)}$. Maintaining the rake angle and clearance angle unchanged, the extended rake and flank surfaces of the fresh tool converge at an imaginary point-A'. Two reference planes, namely the radial plane (π_R) and the tangential plane (π_T) also coincide at this apex point-A. A reference circle (blue dotted line) is also assumed in such a way that it passes through the apex and its centre coincides with the tool axis (Fig. 2c). This reference circle represents the outer diameter for a perfectly sharp tool (edge radius is theoretically zero). However, owing to the presence of a small edge radius, the actual circle based on the outer diameter of the micro-tool (red dotted line) deviates slightly from the reference circle.

After experiencing gradual abrasive wear (Fig. 2b), radius of the same cutting edge increases to $r_e^{(W)}$ where $[r_e^{(W)} > r_e^{(F)}]$. Initially, it is assumed that both the cutting edges of the tool are subjected to equal degree of wear so that initial and final edge radii are identical for both the edges. Later on, the analysis is extended to non-uniform wear scenario as well. For this uniformly worn-out tool, the apex point-A and the reference circle remain unchanged. However, the outer diameter circle of this worn-out tool now passes through point-F. Therefore, there is a reduction in outer diameter of the micro-mill owing to the above-mentioned increase in edge radius caused by abrasion wear. For a given tool engaged in micro-milling, the reference circle has a fixed diameter D_R whereas the outer diameter circle has a variable diameter D_C where $(D_R > D_C)$. The reference circle and the outer diameter circle can also be considered as two concentric circles. As the tool experiences wear with the increase in length of cut, this outer diameter D_C reduces. To geometrically evaluate such reduction in diameter, first the comparison is made between a perfectly sharp tool and the worn-out tool. AH and AN are two tangents for the small circle constituted by the rounded cutting edge (Fig. 2b), and thus $MH \perp AH$ and $MN \perp AN$. So the transient angle $\angle HAM = \angle NAM = \theta_1$ can be expressed in terms of clearance angle (α_O) and rake angle (γ_O) in the following manner.

$$\theta_1 = \frac{1}{2}(90^\circ - \gamma_O - \alpha_O) \tag{2}$$

Now, from the right-angled triangle ΔAHM, the lengths AH and AM can be expressed in terms of edge radius in the following way.

$$AH = \frac{r_e^{(W)}}{\tan\theta_1} = \frac{r_e^{(W)}}{\tan\left(\frac{90^\circ - \gamma_O - \alpha_O}{2}\right)} \tag{3}$$

$$AM = \frac{r_e^{(W)}}{\sin\theta_1} = \frac{r_e^{(W)}}{\sin\left(\frac{90^\circ - \gamma_O - \alpha_O}{2}\right)} \tag{4}$$

From point-M, a vertical line parallel to the plane π_R is drawn that intersects the plane π_T at point-B. This line BM intersects the reference circle at point-D, and the edge radius circle at point-F. Since this point-F is the far most point from the axis of the worn-out tool, the actual outer circle of the worn-out tool also passes through this point-F. Now consider the right-angled triangle ΔABM to represent the lengths AB and BM in the following form.

$$AB = AM\cos(\alpha_O + \theta_1) = r_e^{(W)}\frac{\cos(\alpha_O + \theta_1)}{\sin\theta_1} \tag{5}$$

$$BM = AM\sin(\alpha_O + \theta_1) = r_e^{(W)}\frac{\sin(\alpha_O + \theta_1)}{\sin\theta_1} \tag{6}$$

$$\therefore BF = BM - FM = r_e^{(W)}\left[\frac{\sin(\alpha_O + \theta_1)}{\sin\theta_1} - 1\right] \tag{7}$$

To calculate the small length BD, it is necessary to visualize the entire reference circle (Fig. 1d). Both the points A and D lie on this reference circle such that $AZ = DZ = \frac{D_R}{2}$, where D_R is the diameter of the perfectly sharp tool (diameter of the reference circle). Since the length AB is very small as compared to the tool diameter, it is assumed that ABDX constitutes a rectangle. Therefore, the length BD can be obtained from the right-angled triangle ΔDXZ.

$$BD = \frac{D_R}{2} - \sqrt{\left(\frac{D_R}{2}\right)^2 - \left[r_e^{(W)}\frac{\cos(\alpha_O + \theta_1)}{\sin\theta_1}\right]^2} \tag{8}$$

$$\therefore DF = BF - BD = r_e^{(W)}\left[\frac{\sin(\alpha_O + \theta_1)}{\sin\theta_1} - 1\right] - \frac{D_R}{2} + \sqrt{\left(\frac{D_R}{2}\right)^2 - \left[r_e^{(W)}\frac{\cos(\alpha_O + \theta_1)}{\sin\theta_1}\right]^2} \tag{9}$$

This DF length represents the radial distance between the reference circle and the outer diameter circle of the worn-out tool. Not to mention that the outer circle for a fresh tool also deviates slightly from the reference circle owing to the presence of a small edge radius (Fig. 1c). The corresponding deviation can also be obtained by substituting $r_e^{(F)}$ in Eq. (9). Therefore, the net reduction in tool outer diameter (ΔD_C) owing to the increase in edge radius from $r_e^{(F)}$ to $r_e^{(W)}$ can be expressed in the following way (Eq. (10)). Note that the factor 2 is considered to convert radial change into diameter change.

$$\Delta D_C = 2\left\{r_e^{(W)} - r_e^{(F)}\right\}\left[\frac{\sin(\alpha_O + \theta_1)}{\sin\theta_1} - 1\right] + 2\sqrt{\left(\frac{D_R}{2}\right)^2 - \left[r_e^{(W)}\frac{\cos(\alpha_O + \theta_1)}{\sin\theta_1}\right]^2} - 2\sqrt{\left(\frac{D_R}{2}\right)^2 - \left[r_e^{(F)}\frac{\cos(\alpha_O + \theta_1)}{\sin\theta_1}\right]^2} \tag{10}$$

Eq. (10) can be used to obtain the outer diameter reduction (ΔD_C) from the known values of edge radii before and after micro-milling. Conversion in reverse way is also theoretically feasible, and the intended formula can be obtained by rearranging Eq. (10) in the form of Eq. (11). Although it is theoretically feasible to retrieve edge radius increment from measured values of diameter reduction, from the practical point of view it is an imprecise approach, as discussed below.

$$r_e^{(W)} = \frac{2C_1C_4 - \sqrt{(C_1C_4)^2 - 4\left(C_1^2 + C_2^2\right)\left(C_4^2 - D_R^2\right)}}{4\left(C_1^2 + C_2^2\right)} \tag{11}$$

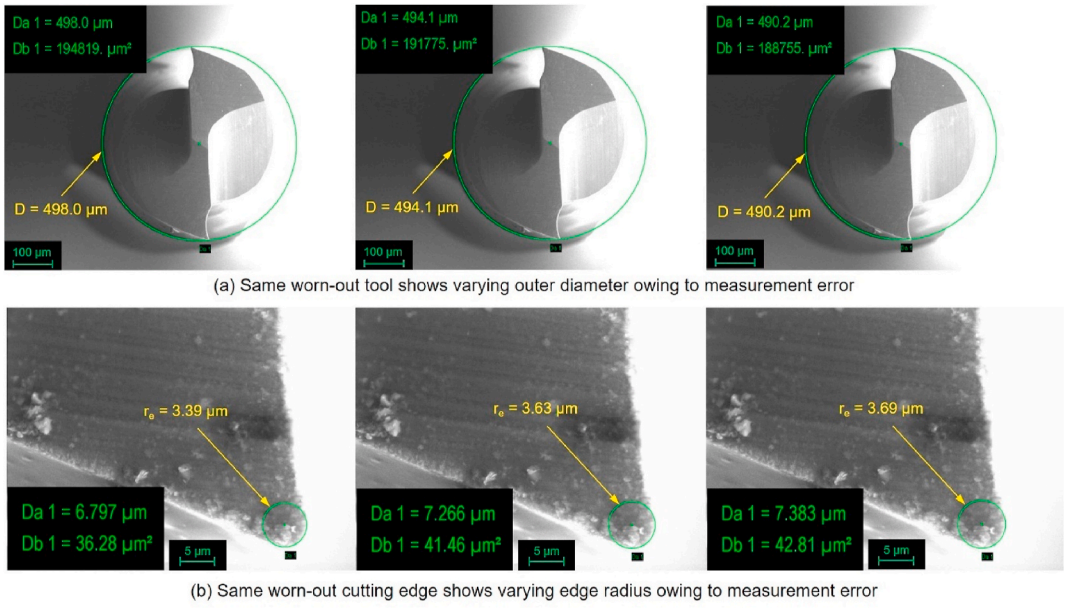

Fig. 3. Scanning Electron Microscope (SEM) images with measured diameter of (a) a particular worn-out tool in three repetitions, and (b) a particular worn-out cutting edge in three repetitions that typically highlight the inherent measurement error.

Where, $C_1 = \left[\frac{\sin(\alpha_O+\theta_1)}{\sin\theta_1} - 1\right]$, $C_2 = \frac{\cos(\alpha_O+\theta_1)}{\sin\theta_1}$, $C_3 = 2\sqrt{\left(\frac{D_R}{2}\right)^2 - \left[r_e^{(F)}\frac{\cos(\alpha_O+\theta_1)}{\sin\theta_1}\right]^2}$,

and $C_4 = \Delta D_C + 2C_1 r_e^{(F)} + C_3$.

For a micro-tool, outer diameter is commonly measured by observing the bottom-view of the tool under a microscope at low magnification (for example, 40–300X for 500 µm tool). Dimension measurement at low magnification is always associated with significant measurement error. Typical measurement error in outer diameter measurement is also shown through scanning electron microscope (SEM) images of a particular worn-out tool (Fig. 3a). Measurement of outer diameter of the same worn-out tool is repeated three times, and three widely varying diameter values (498.0 µm, 494.1 µm, and 496.1 µm) are obtained.

For measuring a tool diameter of 500 µm, the measurement error can reach typically up to ±10 µm. During measuring a dimension of 500 µm, a measurement error of ±10 µm may appear insignificant and tolerable as the corresponding percentage error is only about ±2%. However, when the same measurement error is tallied with respect to tool-life criteria, the measurement error becomes significant and unacceptable. Even if a maximum of 50 µm diameter reduction is considered as the tool-life criteria for a 500 µm micro-mill, ±10 µm measurement error is equivalent to ±20% error in specifying tool-life. Given the short life of the costly micro-milling tools, ±20% error in tool-life might be considered too high. A lower tool-life criterion in terms of diameter reduction further increases the percentage of error. In addition to the erroneous tool-life specification, the inconsistency caused by the widely varying measured values of the outer diameter further introduces difficulty in modelling and analysis of progressive tool wear. Such inconsistency is discussed in detail in section-4. Thus, direct measurement of tool outer diameter during progressive tool wear analysis is an imprecise approach.

On the other side, measurement of edge radius is usually carried out by observing the bottom-view of the tool-edge at high magnification under the microscope. For measuring an edge radius having dimension typically in the range of 0.5–3.0 µm, a high magnification in the order of 3000–5000X (sometimes even higher) is used. It is indeed true that such a measurement technique is also inherently associated with the measurement error; however, its consequence is relatively less severe. As typically shown in Fig. 3b, edge radius of a particular worn-out cutting edge is measured three times, and three different radius values (3.39 µm, 3.63 µm, and 3.69 µm) are obtained. While measuring a worn-out tool edge radius of the order of 10 µm, a measurement error of up to ±1.0 µm can occur. Since 25–30 µm edge radius is considered as the tool life criteria (Table-1), such measurement error is equivalent to 3–4% error in specifying tool life. However, when the measured Δr_e is converted to

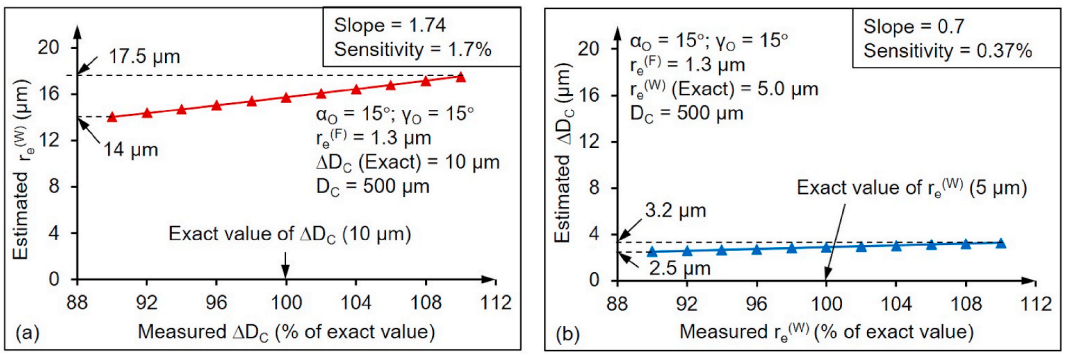

Fig. 4. Influences of the measurement error for a typical set of parameters: (a) variation of estimated edge radius when measured outer diameter reduction falls within 90–110% of the corresponding exact or actual value (application of Eq. (11), and (b) variation of estimated outer diameter reduction when measured edge radius falls within 90–110% of the corresponding exact value (application of Eq. (10)).

ΔD_C through Eq. (10), the measurement error associated with edge radius further transforms to a negligible error (below 1% of the tool life) in diameter reduction.

The sensitivity of measurement error of one parameter on another one is highlighted through Fig. 4. Fig. 4a typically shows the consequence of the measurement error of outer diameter reduction (ΔD_C) on the worn-out edge radius $r_e^{(W)}$ for a particular set of feature values. A measurement error of ±10% is considered that means the measured ΔD_C falls within 90–110% of the corresponding exact or actual value. For this measurement error, the edge radius changes relatively more steeply with an average slope of 1.74. On the contrary, same percentage of measurement error in the edge radius does not change the ΔD_C considerably (Fig. 4b). The sensitivity data also reveals that edge radius is highly sensitive to the fluctuation of ΔD_C value. However, ΔD_C is considerably less sensitive to the $r_e^{(W)}$ value. Therefore, retrieving $r_e^{(W)}$ from measured ΔD_C values using Eq. (11) is associated with considerable error and thus its application is discouraged. Conversely, micro-milling tool-wear related analysis can be carried out in a more precise way if edge radius increase (Δr_e) is practically measured and the corresponding diameter reduction (ΔD_C) is retrieved analytically through Eq. (10).

Fresh micro-mill typically has edge radius in the order of 0.1–0.5% of the tool diameter. As highlighted by Varghese et al. (2021) [16], worn-out tool edge radius of just 5–6% of the tool diameter can be considered as significant enough for inducing high forces, thick adhesion, non-cutting passes, and also catastrophic failure. Considering maximum 8% of the tool diameter as the regime of interest for $r_e^{(W)}$, the variation of ΔD_C against $r_e^{(W)}$ for different tool diameters is shown in Fig. 5a. For a given tool diameter, ΔD_C increases with the edge radius of the worn-out tool. However, the rate of increase in ΔD_C is higher for lower values of the $r_e^{(W)}$. Moreover, a larger tool experiences a larger reduction in diameter for the same set of initial and final edge radii. This variation is more perceptible for higher $r_e^{(W)}$ values and can be clearly observed from Fig. 5b. For a given set of initial and final edge radii, ΔD_C initially increases steeply with the increase in tool diameter. However, it gradually saturates when the worn-out tool edge radius falls below 4% of the tool diameter. In other words, ΔD_C does not vary appreciably so long as the worn-out tool edge radius remains less than 4% of the tool diameter.

For a given set of initial edge radius and tool diameter, ΔD_C also varies with the rake angle (γ_O) and clearance angle (α_O) as well (Fig. 5c). The rake angle (positive, zero, or negative) has negligible influence on the reduction of diameter for the increase in edge radius. With the increase in rake angle from negative (−10°) to positive (+20°) for a constant clearance angle, ΔD_C increases marginally (~15%). On the contrary, clearance angle has significant impact on ΔD_C. For a 500 μm diameter tool, about 515% higher ΔD_C is observed when clearance angle is increased from +5° to +20° keeping initial and final edge radii unchanged. Thus, it can be inferred that, for the same set of initial and final edge radii, a tool with higher clearance angle exhibits more reduction in diameter as compared to a tool having lower clearance angle.

2.2. Non-uniform abrasive wear of the two-flute micro-mills

In practical scenario, both the cutting edges may not necessarily experience similar abrasion. Accordingly, radii of all cutting edges of a worn-out tool may not be same. During micro-milling using an 800 μm two-flute cutter, Oliaei et al. (2016) [17] observed that the radius of one edge increased to 20 μm while the radius of the other edge remained 12 μm after substantial duration of cutting. Apart from the worn-out edge radii, the initial radii for all of the cutting edges of the fresh tool may not necessarily be same as well [18]. For such non-uniform wear scenario, reduction in diameter can be calculated by individually considering the cutting edges (Fig. 6b). For a two-flute micro-mill with non-uniform fresh edge radii $r_{e,1}^{(F)} \neq r_{e,2}^{(F)}$ and non-uniform worn-out edge radii $r_{e,1}^{(W)} \neq r_{e,2}^{(W)}$, an average diameter reduction can be obtained in the following manner.

$$\Delta D_{C,avg} = \frac{[\Delta D_C]_{r_{e,1}^{(F)} \rightarrow r_{e,1}^{(W)}} + [\Delta D_C]_{r_{e,2}^{(F)} \rightarrow r_{e,2}^{(W)}}}{2} \tag{12}$$

When the average diameter is considered, the centre of the outer circle of the non-uniformly worn-out tool slightly shifts from the actual

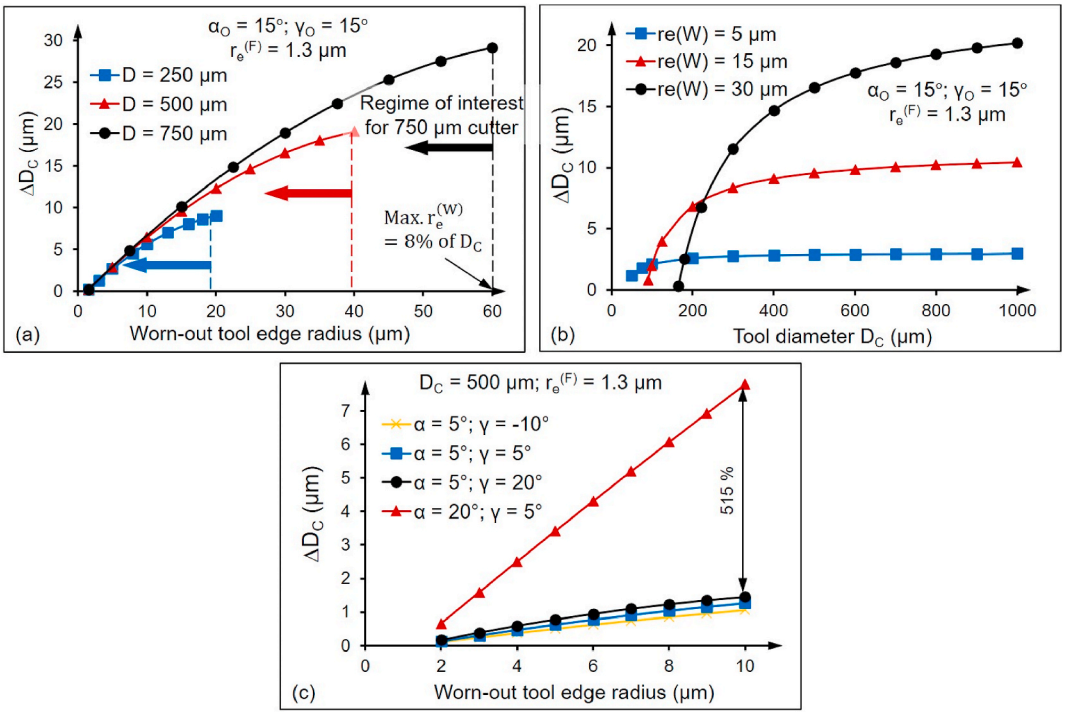

Fig. 5. Typical plots showing the effects of various features of the worn-out cutting edge on the outer diameter reduction.

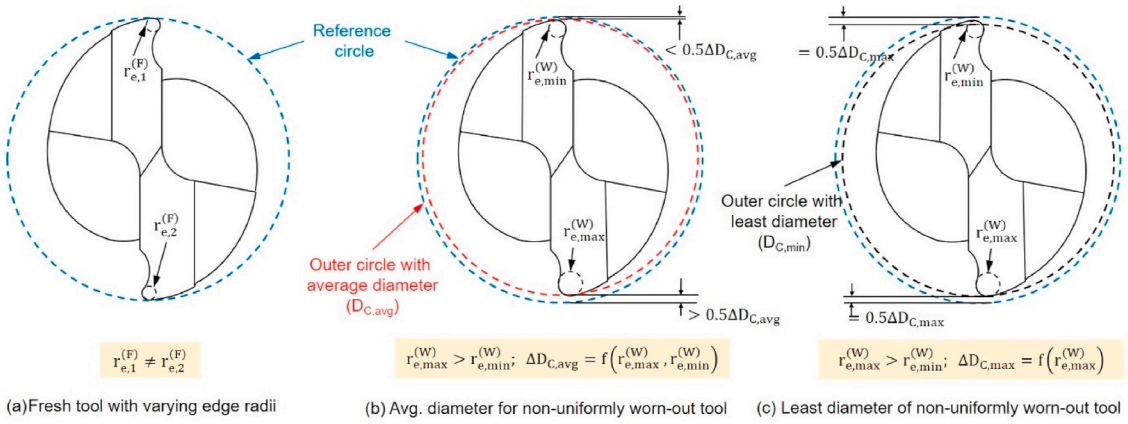

Fig. 6. Measurement of average diameter and least diameter for non-uniformly worn-out tool.

tool axis leading to eccentricity problem. Instead of using an average wear, maximum wear is been conventionally taken into consideration for tribological analysis. With micro-milling tool, if maximum wear is only given weightage, then the corresponding outer circle passes through the tip of the worn-out edge having larger radius (Fig. 6c). In such a scenario, the other worn-out edge with smaller edge radius is given no weightage. The maximum reduction in diameter can be obtained in the following manner (Eq. (13)). It is obvious that $\Delta D_{C,max} > \Delta D_{C,avg}$. Accordingly, the outer diameter estimated following the maximum wear strategy becomes lower than that obtained through average wear method.

$$\Delta D_{C,max} = [\Delta D_C]_{r_e^{(F)} \rightarrow r_{e,max}^{(W)}} \tag{13}$$

2.3. Effect of material adhesion on the cutting edges

Adherence of the workpiece or chip material on the cutting edge is another common type of wear experienced by the micro-milling tools [19]. However, the formation, growth, and disappearance of such adhesive deposits occur without any external influence during the machining process. Thus adhesive deposits neither contribute to the tool core strength nor alter the geometry of the actual cutting edge. Distinguishing the adhered material from the actual cutting edge is not feasible by observing the tool at low magnification. The same can, however, be performed with a greater degree of accuracy by observing individual cutting edge at higher magnification. Once the actual edge is distinguished, a circle can be fit to measure radius (Fig. 7a), and thereafter, ΔD_C can be estimated following Eq. (10). Note that the directly measured ΔD_C value for an adhered tool is expected to fetch an erroneous value as such measurement is carried out at a low magnification where adhered material cannot be distinguished from the actual edge. In direct measurement of diameter of an adhered tool, only apparent diameter can be measured, rather than the diameter of the actual tool. Thus observing the individual edges for measuring actual edge radius, and subsequently estimating the outer diameter is a more precise approach.

2.4. Effect of edge chipping

The severe form of wear a micro-milling tool experiences is the edge-chipping. As schematically shown in Fig. 7b, a portion of the tool-tip breaks away catastrophically leading to micro-chipping. Cutting edge also loses its sharpness significantly. For such a chipped tool, the edge radius cannot be measured accurately as the edge loses its roundness owing to flank flattening. Instead, flank wear length (V_B) is one crucial parameter for quantitative wear analysis for such chipped tools. The reduction in outer diameter of the cutter post-chipping can also be estimated using the flank wear length and other relevant tool angles. Note that the measurable V_B length is actually the projected length between points P and Q on the tangential plane (π_T). Since the outer

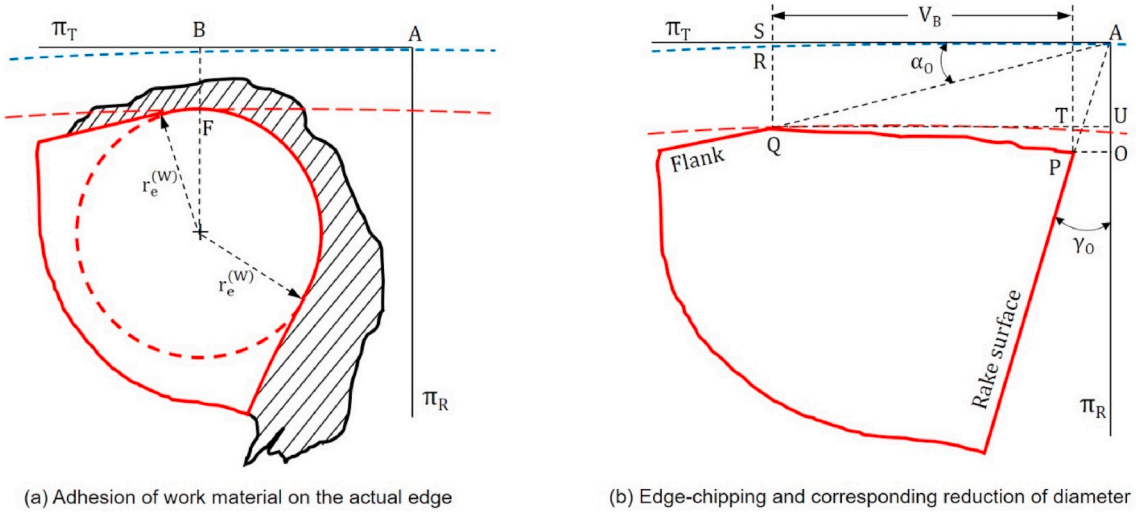

Fig. 7. Schematic representation of the cutting edge (a) with adhered workpiece material, and (b) after brittle fracture in the form of micro-chipping.

diameter circle now passes through point-Q, the intended ΔD_C is twice the length RQ. For geometrical evaluation, a line QU perpendicular to the radial plane (π_R) is first taken such that $AS \cong (V_B + SQ\tan\gamma_O)$. From the right-angled triangle ΔAQS, the length SQ can be expressed in the following form.

$$SQ = \frac{V_B \tan\alpha_O}{1 - \tan\alpha_O \tan\gamma_O} \tag{14}$$

The small length SR can be calculated in a similar way as discussed in section-2.1 through Fig. 2d focusing on the entire reference circle. In terms of flank wear length (V_B), the SR can be expressed as follows.

$$SR = \frac{D_R}{2} - \sqrt{\left(\frac{D_R}{2}\right)^2 - \left(\frac{V_B}{1 - \tan\alpha_O \tan\gamma_O}\right)^2} \tag{15}$$

Therefore, the outer diameter reduction (ΔD_C) owing to a flank wear length of V_B can be expressed through the twice of RQ as given below.

$$\Delta D_C = \left(\frac{2V_B \tan\alpha_O}{1 - \tan\alpha_O \tan\gamma_O}\right) - D_R + \sqrt{D_R^2 - \left(\frac{2V_B}{1 - \tan\alpha_O \tan\gamma_O}\right)^2} \tag{16}$$

3. Experimental details

TiAlN-coated tungsten carbide (WC/6Co) micro end mill (AXIS-Microtools) of 0.5 mm diameter is used for validation purpose (Fig. 5a). The rake angle and clearance angle of this tool are 11.25° and 20°, respectively. This micro-cutter consists of two helical flutes (two cutting edges) with 30° helix angle and 1.5 mm effective flute length. Useful features of the micro-mill are given in Table-2. Compositions of the tool coating and substrate materials are also given in Table-3 and Table-4, respectively. Although insignificant, the non-uniformity in edge radii among the two cutting edges of the fresh tool with $r_{e,1}^{(F)} = 1.34\ \mu$m and $r_{e,2}^{(F)} = 1.38\ \mu$m can be noticed from Fig. 8. This non-uniform nature of the cutting edge radii of the fresh tool is taken into account for further analysis. To distinctly identify two cutting edges throughout the experiments, a suitable marking is put on the tool shank.

This tool is used for micro-milling of difficult-to-machine Ti–6Al–4V titanium alloy (Table-5). A 5.0 mm wide flat island is initially created on the workpiece, and thereafter, full-immersion straight slots are micro-milled on this island with side-entry and side-exit of the cutter. Thus each micro-slot is 5.0 mm long and 0.5 mm wide. The entire set of micro-milling experiments is carried out on the KERN-Evo ultra-precision micro-machining centre (KERN microtechnik) using a constant spindle speed of 45,000 rpm, feed per flute of 4.0 μm/flute and axial depth of cut of 40 μm. For 0.5 mm diameter cutter, this rotational speed transforms to 70.7 m/min cutting velocity. An approach and overtravel of 1.0 mm each is also considered. Accordingly, micro-milling of one 5.0 mm long slot takes about 1.17 s where each cutting edge ideally engages and disengages 625 times with the workpiece. A commercial eco-friendly (biodegradable) cutting fluid UNILUBE 2032 (UNILUBE AG) [20] is also delivered at 6 mL/h oil flow rate using two nozzles following sustainable minimum quantity lubrication (MQL) strategy using an inbuilt ECOLUBE dispenser facility. Nozzles are placed behind the tool along the tool-feed direction with an intent to lubricate the trailing edges by depositing the MQL oil droplets directly on the edge during the corresponding disengagement period [21].

Table-2
Features of the fresh micro-milling tool.

Property	Value
Cutting tool	Two-flute flat-end micro-mill
Cutter diameter	498 μm
Helix angle	30°
Rake angle	11.25°
Clearance angle	20°
Edge radii	1.34 and 1.37 μm
Coating material	TiAlN
Substrate material	WC/6Co

Table-3
Composition of the tool-coating material (TiAlN).

Element	Ti	Al	N
Composition (wt %)	38.93	29.77	31.30

Table-4
Composition of the tool-substrate material (WC/6Co).

Element	W	C	Co
Composition (wt %)	71.72	22.10	6.18

Tool condition is inspected after every 5 mm length of cut by observing the tool under a scanning electron microscope (SEM) (EVO 18, ZEISS). A low magnification (300X) is used for observing the bottom-view of the entire worn-out tool and subsequently measuring the outer diameter. All other features (like edge radius, rake angle, and clearance angle) are measured by individually observing the edges at a high magnification (5000X). Flank wear length is also measured by observing the side-view of the tool (i.e. principal cutting edge) at a similar high magnification. Sometimes SEM images are further processed through AxioVision software for measuring necessary dimensions. The cutting tool is used up to 200 mm length of cut to validate the previously developed analytical equations across various regimes of tool wear. The SEM is also fitted with an energy-dispersive X-ray spectroscopy (EDS) facility, which is also used for measuring elemental composition of a worn-out tool and adhered material. The cleaned micro-milled slots are further scanned using a non-contact type 3-D surface profilometer (CCI MP, Taylor Hobson), and the scanned files are processed through Taly-Map Gold software to retrieve slot width and other surface topographical information.

4. Results and discussion

For retrieving diameter reduction (ΔD_C) from the geometry of the worn-out edges using Eq. (10), the initial task is to calculate the reference diameter (D_R). Although 500 μm diameter tool in as-procured condition is employed during the experimentation, the reference diameter will not be exactly 500 μm owing to the manufacturing error. For precisely obtaining the reference diameter, Eq. (10) can be extended in the form of Eq. (17) to compare between a perfectly sharp tool and the as-procured tool having known edge radius. In such a scenario, $r_e^{(F)} = 0$ (for perfectly sharp tool). Substituting the measured values of the as-procured tool (Table-2), the reference diameter can be found to be $D_R = 499.45\ \mu$m.

$$2D_R - D_C = 2r_e^{(W)}\left[\frac{\sin(\alpha_O + \theta_1)}{\sin\theta_1} - 1\right] + 2\sqrt{\left(\frac{D_R}{2}\right)^2 - \left[r_e^{(W)}\frac{\cos(\alpha_O + \theta_1)}{\sin\theta_1}\right]^2} \tag{17}$$

4.1. Validation in abrasive wear regime

When a fresh micro end milling tool having a very small edge radius is used for machining of hard and difficult-to-machine material (Ti–6Al–4V), the cutter passes through various stages of wear with the progression of micro-milling. Initially the cutting edges predominantly undergo abrasion where the edge radius increases retaining the basic form of the rounded edge. For the experimental condition investigated here, this abrasive wear regime continues up to 85 mm length of cut. Note that chips loosely adhere over the tool body right from the micro-milling of first slot; however, such loosely adhered chips deposit

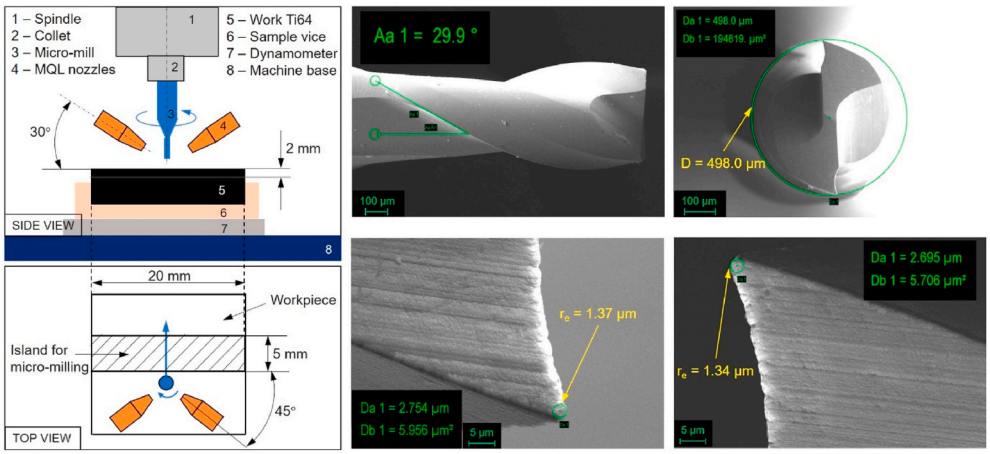

Fig. 8. Schematic of the micro-milling set-up and various features of the fresh micro end milling tool used in this experiment.

Table-5
Composition of the workpiece material (Ti–6Al–4V).

Element	Ti	Al	V	Fe	Cr
Composition (wt %)	89.70	5.87	4.15	0.13	0.04

substantially away from the active portion of the cutting edge (Fig. 9). During micro-milling with a feed of 4 µm/flute, the rounded cutting edge with surrounding rake and flank surfaces up to a length of 10–15 µm comes in direct tribological contact with the workpiece and chip [21]. Thus loose chip adhesion over the tool body away from the active region of the edges does not significantly influence the mechanics of material removal. Strong adhesion on the cutting edge that occurs after 85 mm length of cut is discussed separately in section-4.2.

Gradual increase in edge radius (Fig. 9b) with the progression of

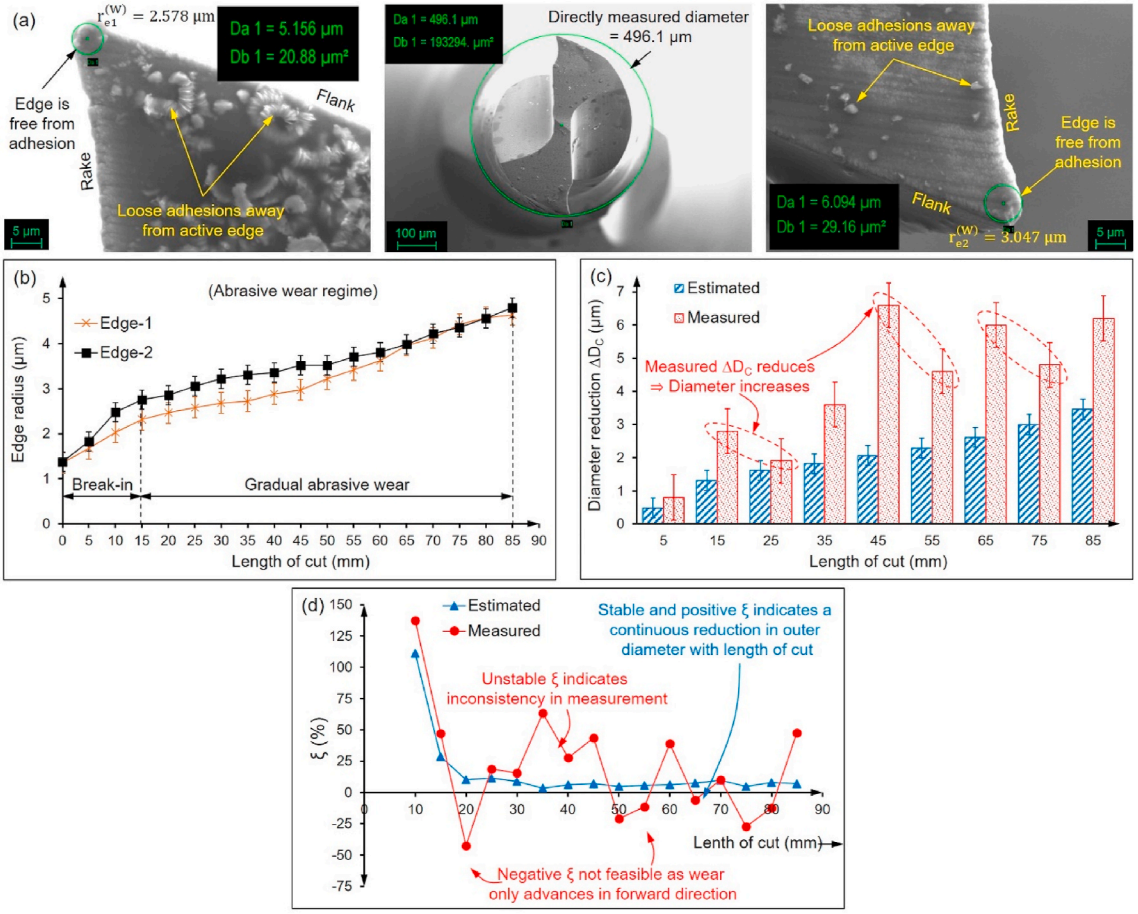

Fig. 9. Abrasive wear regime: (a) typical SEM images of the worn-out tool and subjected to abrasion after 25 mm length of cut with measured dimensions, (b) variation of edge radius of the two cutting edges with the length of cut, (c) bar chart showing the variation of directly measured and analytically estimated diameter reduction values, and (d) inconsistency of the measured and estimated diameter reduction values with progressive micro-milling.

micro-milling within the abrasive wear regime is accompanied by the loss of material from the cutting edges resulting in a decrease in the outer diameter. The estimated reduction of the outer diameter (ΔD_C) that is calculated from the geometry of the worn-out edges shows a continuously and steadily increasing trend with the length of cut (Fig. 9c). By the end of 85 mm cut, the estimated outer diameter reduces by 3.58 μm whereby the radius of the two edges increases to 4.63 μm and 4.79 μm. The directly measured ΔD_C values are affected by inconsistency in measurement that results in the fluctuation of measured values. Such inconsistency in measurement between every 5 mm length of cut can be expressed through a step-change variable. The percentage change of the response variable (ΔD_C in this case) between two consecutive measurements can be expressed through the step-change variable (ξ), as given in Eq. (18), where i indicates measurement trial ($i = 1, 2, 3, \ldots$). Since wear proceeds through forward direction only, a positive value of ξ is always expected.

$$\xi_{i+1} = \frac{(\Delta D_C)_{i+1} - (\Delta D_C)_i}{(\Delta D_C)_i} \tag{18}$$

Among the estimated ΔD_C values, a high ξ is recorded for initial 15 mm length of cut (Fig. 9d). This can be attributed to the rapid break-in wear of the cutting edges at the beginning of machining where the edge radius increases steeply resulting considerable reduction in outer diameter (or increase in ΔD_C values). Edge radii increase steadily but at a relatively low rate beyond this break-in wear zone, and thus, small positive ξ values (5–8%) are recorded for the rest of the abrasive wear regime. This indicates a steady and continuous decrease in outer diameter with the length of cut. On the contrary, the directly measured ΔD_C values initially show a steep increase; however, the same decreased between 15 and 25 mm leading to a negative ξ value. Such negative ξ values are also recorded for few more instances. $\xi < 0$ essentially indicates an increase in the diameter with the length of cut, which is unlikely to occur in abrasive wear regime. Apart from the negative value, the unsteady and haphazard variation of ξ also reflects the lack of consistency among the measured ΔD_C values.

4.2. Validation in adhesive wear regime

When the abrasively worn-out blunt tool is used for further micro-milling, the active portion of the cutting edge starts experiencing strong adherence of chip/workpiece material. Such adhered material can be easily distinguished from the actual cutting edge by observing the edges at high magnification under a microscope, as shown in Fig. 10. For the experimental condition investigated here, adhesive wear without edge-chipping continues for a short length of cut (85–115 mm), after which the chipped-tool experiences adhesion. Such pre-chipping adhesive deposits can change the apparent geometry of the cutting edges without significantly affecting the actual edges. Presence of adhered layer over the original cutting edge helps protecting the tool surface from further loss of material. Accordingly, the radius of the actual cutting edges does not change significantly with the length of cut (Fig. 11a). Since the estimated ΔD_C values are assessed based on the actual cutting edge geometry disregarding the adhesion, the estimated ΔD_C values remain more-or-less unchanged within adhesive wear regime (Fig. 11b).

Directly measured ΔD_C values, however, vary significantly with the length of cut. As the adhered material cannot be distinguished from actual cutting edge in the direct measurement technique, a larger apparent diameter is measured. This is one drawback of the direct measurement technique since the apparent diameter can only be measured, rather than the actual tool diameter. Referring back to Fig. 9c, the measured ΔD_C values are always higher than that of the estimated values in abrasive wear regime. An opposite scenario can be observed in most of the cases within the adhesive wear regime. Owing to the presence of adhered material on the edges, the tool appears larger when observed at low magnification under the microscope. With the growth of adhered layer with machining time, the outer diameter also appears to increase leading to a reduction of ΔD_C value. The step-change variable (ξ) also remains steady and very low (positive) for the estimated ΔD_C values (Fig. 11c). This indicates a consistent rise of ΔD_C though at a very low rate with the length of cut. On the contrary, highly negative ξ for the measured ΔD_C values reflects the inconsistency and unlikely measured data.

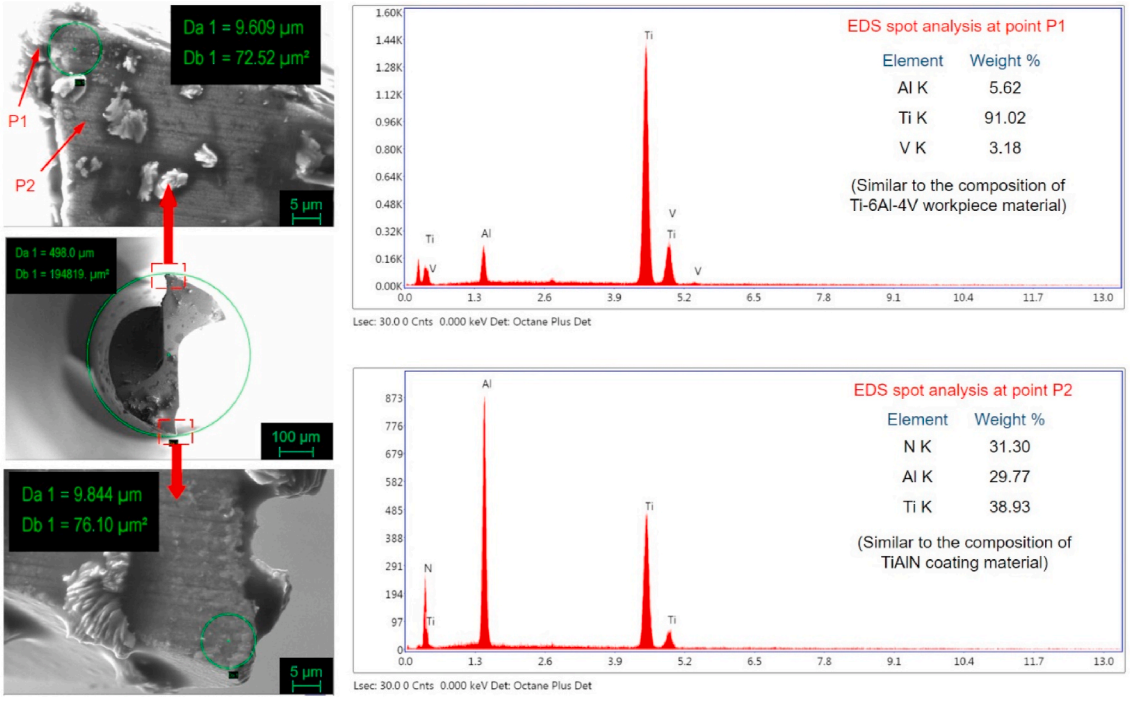

Fig. 10. Adhesive wear regime: apparent diameter (without separating the adhered material) can only be measured in the direct measuring technique, whereas the adhered workpiece material can be separated from actual edge at high magnification measurement of cutting edges (EDS spot analysis result confirms the adhesion of the workpiece material at the edges).

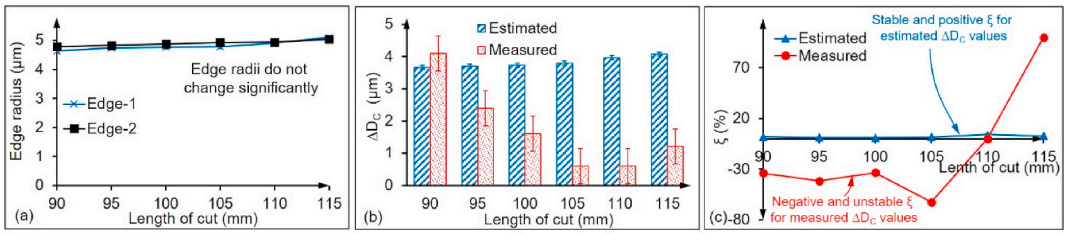

Fig. 11. Adhesive wear regime: variations of the (a) edge radii, (b) measured and estimated values of the outer diameter reduction, and (c) consistency of the measured and estimated diameter reduction values with length of cut.

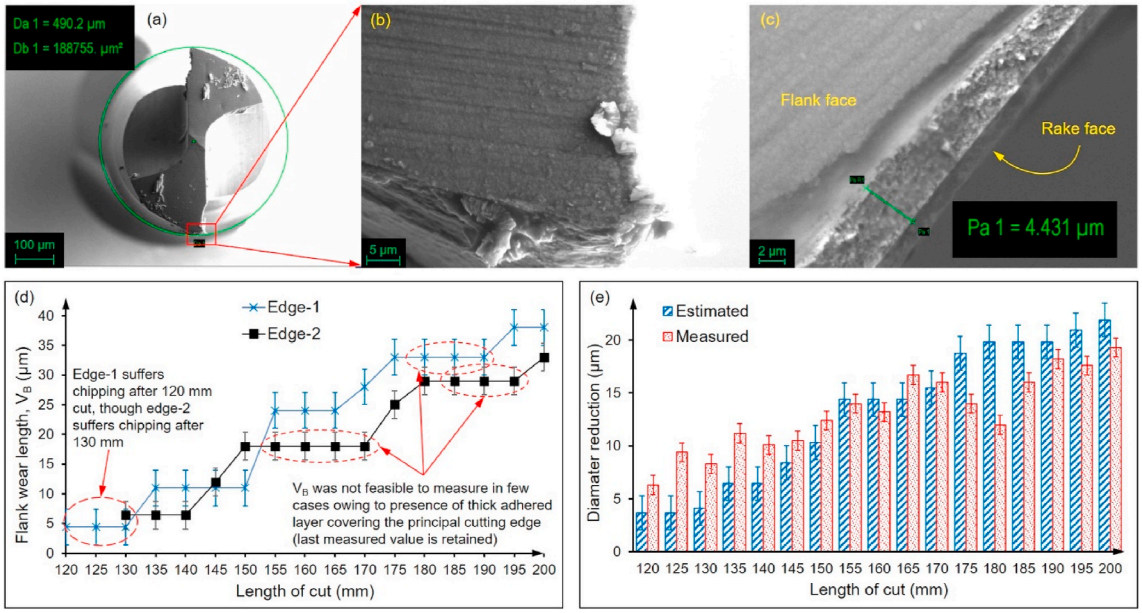

Fig. 12. Edge-chipping regime: (a–b) condition of the tool and edge post-chipping, (c) side-view of the edge with chipped portion, (d) variation of flank wear length with length of cut, and (e) variation of estimated and measured values of the outer diameter.

4.3. Validation in edge-chipping regime

After the short adhesion regime, the cutting edges undergo brittle fracture leading to micro-chipping. As a tiny portion of the tool-tip breaks away, the roundness property of the edge is lost. Thus fair measurement of the edge radius is not feasible once the chipping took place. Flank wear length (V_B) that can be measured from the projected view of the principal cutting edge (Fig. 12) is an appropriate index for quantitatively expressing tool wear in the chipping regime. It is worth mentioning that both the cutting edges may not necessarily undergo chipping after the same length of cut. Thus the first instance of micro-fracturing in either of the edges is treated as the beginning of chipping regime.

The exposed WC/6Co substrate post-chipping further attracts material adhesion (discussed in detail in section-5). This adhered material protects the edge for certain duration. When the adhered material dislodges, the edge once again experiences micro-chipping leading to further increase in V_B length. For the same reason, the flank wear length (V_B) of each edge cannot be measured at every 5 mm interval (the adhered material covers the chipped portion making it infeasible to measure). Thus the last measured V_B value is retained for such unmeasurable occasions. Accordingly, a monotonically increasing trend of V_B with length of cut cannot be observed; rather a stepped increasing pattern can be noticed (Fig. 12d). However, an increasing trend of V_B with the machining time can easily be perceived for both the edges.

Since the chipping and adhesion occur in a cyclic pattern after 115 mm length of cut, the tools are tested up to 200 mm of machining. As V_B changes with the length of cut, the estimated ΔD_C also changes. The estimated outer diameter of the 500 μm tool reduces by about 22 μm (about 4.4%) at the end of 200 mm length of cut whereby two cutting edges undergo 33 μm and 38 μm flank flattening.

4.4. Variation of the micro-milled slot width

In full immersion slot milling, the width of the slot floor inherently matches with the instantaneous tool diameter [22]. Measuring the width of the slot bottom surface is feasible in two distinct ways, as shown in Fig. 13. For the destructive approach, the micro-milled samples are first sliced using wire electro-discharge machining, and the cross-section of the sliced sample is further finished by polishing and etching to observe under SEM for directly measuring the slot width. This destructive approach is not only time consuming but also associated with inherent measurement error as a dimension of the order of 500 μm is measured at a low magnification. For a faster and more precise measurement of the slot width, the non-destructive approach can be adopted where the cross-sectional profile at an imaginary section can be retrieved by software analysis of the 3D scanned file of the cleaned micro-milled slots as described in Section-3. For the first micro-milled slot (i.e. 0 – 5 mm length of cut), the slot width is measured to be 498.1 μm in destructive approach. For the same slot, the slot width measured by non-destructive approach is found to be 498 μm. Since both the values match closely, the non-destructive approach is adopted for measuring slot width for rest of the slots.

As the tool outer diameter reduces owing to progressive wear, the

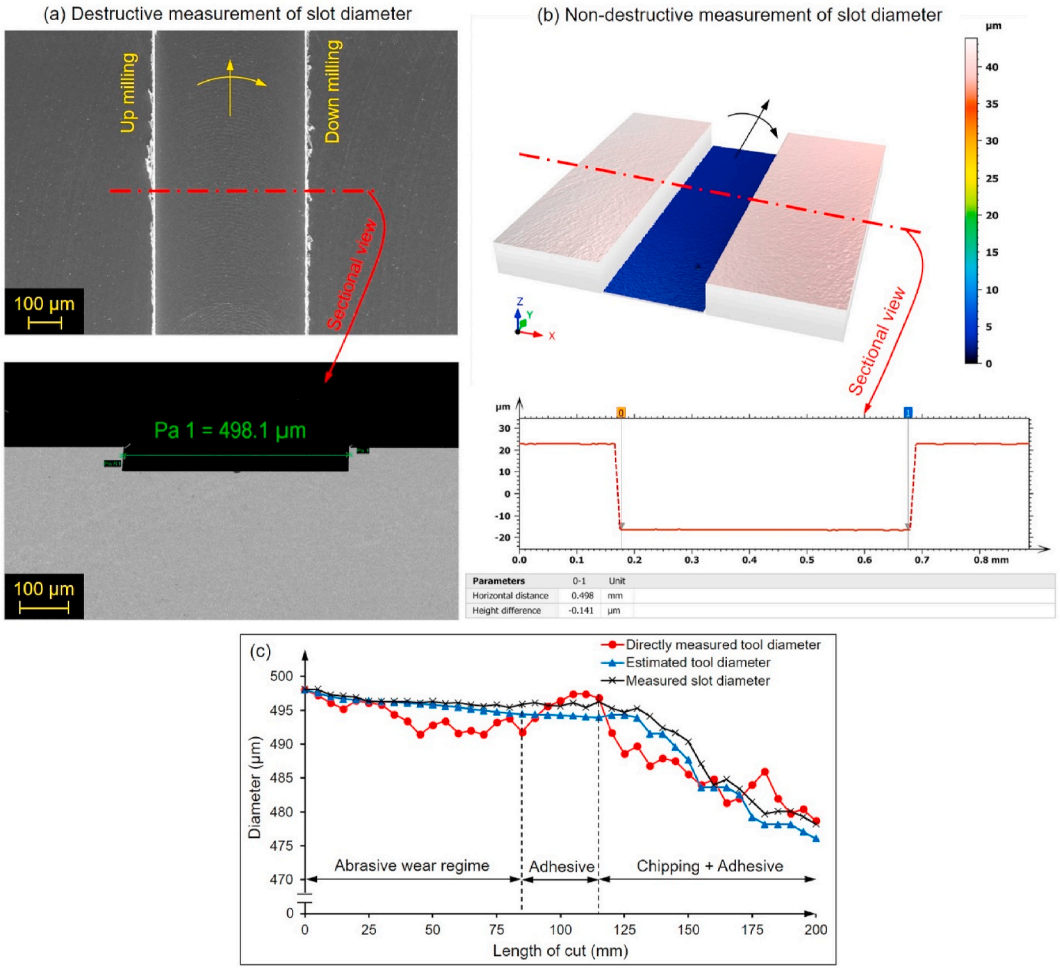

Fig. 13. Micro-milled slot width: (a) destructive measurement approach where samples are sliced and polished, and cross-section is observed using SEM to measure slot width, (b) non-destructive measurement approach where the sectional view is obtained through software analysis on the 3D scanned file, and (c) the variations of measured slot width, measured tool diameter, and estimated tool diameter with the length of cut.

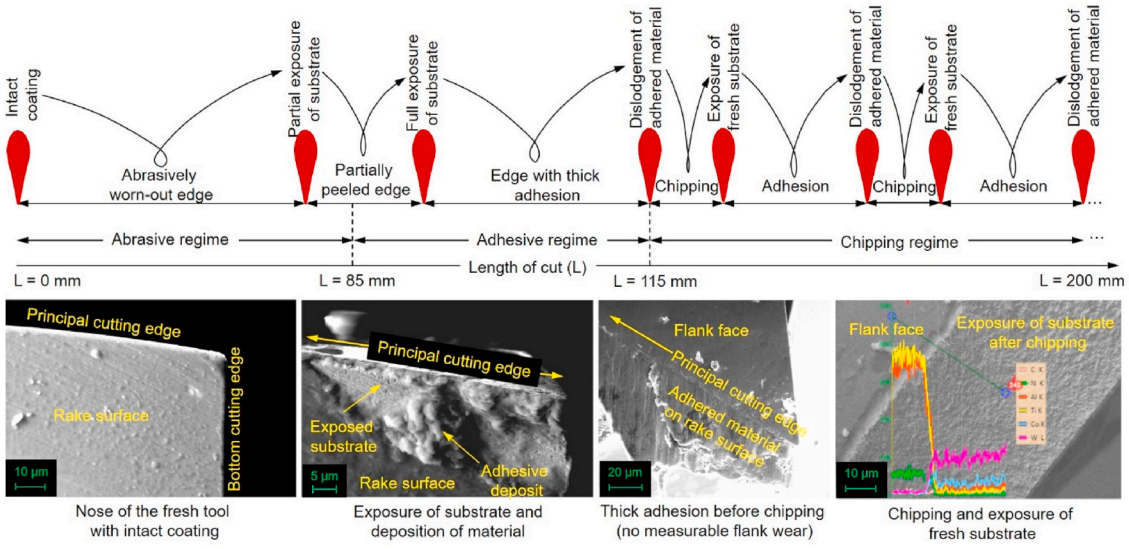

Fig. 14. A flow diagram that represents the progression of micro-milling tool wear across various stages (typical SEM images of few events are also given).

slot width also decreases gradually with the length of cut. Within the abrasive wear regime, the slot width matches closely with the estimated tool diameter. Unlike the directly measured tool diameter, the slot width reduces gradually and consistently. In the short adhesive wear regime, the slot width also varies following the pattern of estimated tool diameter. However, the slots are somewhat wider than the tool diameter. The work-hardened adhered material at the cutting edge tends to plough the workpiece material leading to the generation of slightly wider slot as compared to the actual tool diameter. However, the slots are not as wider as the directly measured tool diameter. Furthermore, a consistent variation in slot width is also recorded in adhesive wear regime too.

In the chipping wear regime, the pattern of variation of the slot width closely follows the trend of the reduction of estimated tool diameter. However, the stepped decrease in estimated tool diameter (or stepped increase of ΔD_C as in Fig. 12) is not reflected in slot width. This is because the ΔD_C values in chipping regime are estimated from corresponding V_B values, and the last measured value is preserved for non-measurable occasions, as discussed in Section-4.3. Unlike flank wear length, the slot width can be measured in all of the trials using the non-destructive approach. Hence, a consistent variation of the slot width instead of a stepped variation is recorded. Similar to that observed in adhesive regime, the slots in chipped regime are somewhat wider than the estimated tool diameter owing to the presence of adhered layer over the chipped edge in most of the times. Nevertheless, a consistent and steady decrease of the slot width can be noticed that closely follows the trend of the estimated tool diameter.

5. Mechanism of tool wear with the progression of micro-milling

Gradual wear of the cutting tool is inevitably associated with micro-milling owing to the presence of relative velocities under high contact pressure between the chip-tool-workpiece. When a fresh micro-mill with a small edge radius is engaged for machining, initially it experiences uniform abrasive wear leading to the increase in edge rounding (Fig. 14). The edge retains its rounded shape even though the corresponding radius increases. Occasional loose adherence of the chip over the entire tool body also occurs; however, the active portion of the edges remains more-or-less free from such adherence. Thickness of the coating layer over the cutting edge also slowly decreases with the continuation of abrasion. Gradually, a stage arrives when WC/6Co substate starts exposing. Sudden delamination caused by the abrupt peeling off of the coating layer usually does not occur owing to very small shear forces. Instead, thickness of the coating layer gradually decreases leading to nonuniform exposure of the substrate towards the end of the abrasive wear regime. With the further increase in length of cut, complete exposure of the substrate occurs that establishes the onset for strong adhesion.

The workpiece material at the cutting zone comes in direct tribological contact with the exposed substrate after the delamination of the coating. Accordingly, the tribo-contact pair shifts from Ti64–TiAlN to Ti64-WC/6Co (i.e. from workpiece-coating to workpiece-substrate). Strong chemical affinity between Ti–6Al–4V and tungsten carbide [23] promotes quick adherence of workpiece material on the exposed cutting edge (mainly rake surface) in the form of thick built-up edge (BUE). The micro-hardness (or abrasion resistance) of the WC/6Co substrate is substantially higher than that of Ti–6Al–4V; however, the former one has relatively lower hardness than that of TiAlN coating. Accordingly, the exposed substrate is expected to experience steeper wear rate post-delamination. Contrary to that, a relatively lower wear rate is observed in the adhesive wear regime (Fig. 11) as compared to that in the abrasive wear regime (Fig. 9). The adhered layer of the workpiece material over the cutting edge itself acts as the sacrificial layer and thereby protects the substrate from experiencing steeper abrasion.

Cutting temperature in micro-milling remains reasonably low owing to very small feed per flute and depth of cut. In addition, each cutting edge simultaneously engages and disengages with the workpiece in every tool rotation. The inherently intermittent type cutting process allows heat dissipation from the edges during the disengagement period. By placing thermocouples, Wang et al. (2019) [24] measured a maximum of about 70 °C temperature rise of the workpiece during micro-milling of Ti–6Al–4V. Using simulation, Wang et al. (2020) [25] also recorded a maximum cutting zone temperature of about 180 °C in dry micro-milling of same alloy. Apart from the low cutting temperature, the tribo-contact duration between an edge and the workpiece also remains very small, in the order of 6.6×10^{-4} seconds per rotation (for 45, 000 rpm). Low rise in temperature in conjunction with very short period of tribo-contact fails to induce thermally sensitive wear modes (such as plastic bulging, thermal fracture, flaking, diffusion, etc.) during micro-milling using TiAlN coated WC/6Co tools. Thus, micro-milling tools predominantly encounter mechanical modes of wear.

As the edge radius (r_e) increases with the length of cut, the minimum uncut chip thickness (h_{min}) also increases proportionally [26]. The volume fraction of the workpiece material undergoing ploughing (elastic-plastic deformation) is proportional to h_{min}. On the other hand, the volume fraction of the workpiece material undergoing shearing (chip formation) is proportional to $(f_z - h_{min})$ [27]. Note that the set feed per flute (f_z) remains unchanged (so maximum uncut chip thickness is constant). Accordingly, as h_{min} increases with the machining time, the volume fraction of the material susceptible to ploughing increases whereas the volume fraction of shear-prone material decreases. When h_{min} becomes substantially high, each cutting edge in every tool rotation fails to shear off workpiece material in the form of chip. Instead, the tool itself bends in opposite direction of tool-feed allowing accumulation of uncut chip material ahead of it. This leads to the generation of non-cutting passes. The entire accumulated chip is then removed in a single stroke in a subsequent cutting pass. Such cutting and non-cutting passes repeatedly occur when the edge radius of a worn-out tool becomes substantially higher than the set feed per flute. This scenario can be detected from the developed lay marks (feed marks) at the bottom surface of the micro-milled slot.

As shown in Fig. 15, the bottom surface generated at the beginning of micro-milling is characterized by uniformly and homogeneously distributed lay marks. This is the indication of material removal by each cutting edge in every tool rotation. Occasional non-cutting passes can be observed towards the end of adhesive wear regime where edge radius increased to about 5.0 μm. However, in the chipping regime with thick adhesion on the edge, the process is dominated by repeated non-cutting passes. The corresponding lay marks at the bottom surface becomes completely uneven and non-homogeneous. The non-cutting passes tend to completely smear the surface owing to repeated rubbing with the previously generated lay marks. This inherent planarization effect tends to flatten the lay marks leading to the generation of apparently smooth surface (absence of scallops). However, when the accumulated uncut material is removed in a cutting pass followed by multiple non-cutting passes, material pile-up occurs leading to the occasional generation of significantly higher asperities.

Non-cutting passes undesirably increase the chip load (proportional to thickness of the uncut chip) for the subsequent cutting pass. Accordingly, during a cutting pass, the corresponding active edge experiences significantly high forces and stresses capable of inducing micro-fracturing. Of the entire rounded cutting edge, a small portion at the tool-tip having thickness h_{min} experiences plastic deformation of the workpiece material; and hence, this portion of the edge experiences significantly higher stresses (specific ploughing energy is substantially higher than specific shearing energy) [28]. Accordingly, the tool-tip of thickness h_{min} corresponding to the radius of worn-out edge is susceptible to brittle fracture in the form of edge chipping. Thus, chipping occurs after the exposure of the substrate and is induced by the non-cutting passes at high edge radius of the worn-out tool. Upon chipping, fresh area of the WC/6Co substrate exposes that once again attracts workpiece material leading to further adhesion. This adhered

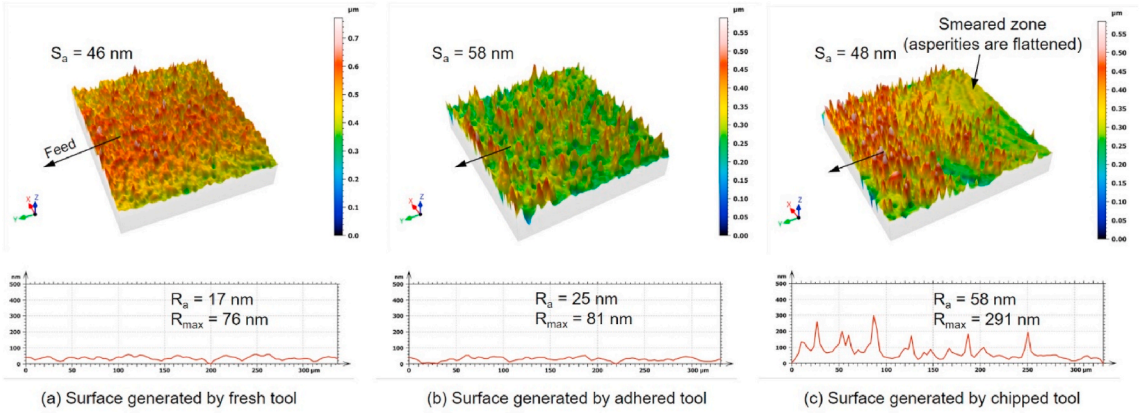

Fig. 15. Non-contact type scanned profiles (3D areal and 2D sectional) of the bottom surface of the micro-milling slot generated by (a) fresh, (b) adhered, and (c) chipped edges.

material protects the actual edge for a small duration of machining. Once the adhered material partially or completely dislodges, the substate again tends to undergo micro-chipping. Such repetition of chipping and adhesion continues for a significantly longer length of cut. Complete catastrophic breakage of the tool usually does not take place even within 500 mm length of micro-milling. However, the tool life may be considered to have been exhausted much before the catastrophic breakage owing to degraded machinability and poor accuracy [25,29] of the micro-milled feature.

6. Diameter reduction as an index for tool life assessment

In macro-scale machining, the flank wear length is conventionally used as the index for assessing tool life. However, in micro-milling, so far researchers have used different indexes, such as edge radius, flank wear length, and diameter reduction, for defining the criteria for the exhaustion of useful service life of the tool (Table-1). For drawing a tool life curve, it is necessary to use such a quantifiable variable that increases uninterruptedly from the beginning of machining until the point of inflexure. In this section, an attempt is made to explore the feasibility of using outer diameter reduction (ΔD_C) as the variable for drawing tool life curve for micro-milling.

As discussed earlier in sections 2.1 and 2.3, the cutting edge of the micro-milling tool retains its rounded shape throughout the abrasive and adhesive wear regimes. So edge radius can be considered as an appropriate parameter for drawing tool life curve; however, the same cannot be extended in the chipping regime as the edge loses its roundness property. After edge-chipping, the flank wear length (V_B) can be used for the same purpose. On the other hand, the same V_B length cannot be detected or measured before chipping occurs. Therefore, neither edge radius nor flank wear length can be consistently employed for drawing tool life curve. Since V_B and r_e are two independent parameters, a clear non-continuity in the tool life curve occurs at the transition zone from adhesive to chipping regimes (Fig. 16).

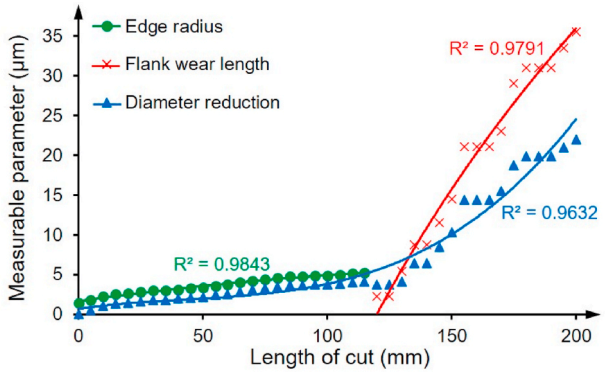

Fig. 16. Feasibility of drawing tool life curve for micro-milling tool using three measurable variables (edge radius of the worn-out tool, flank wear length, and outer diameter reduction).

On the other hand, the outer diameter reduction (ΔD_C) increases uninterruptedly with the length of cut (or machining time) regardless of the wear regimes. The best fit line for the estimated ΔD_C values also shows a reasonably good coefficient of determination ($R^2 = 0.96$). Thus, among the three measurable parameters, ΔD_C can be treated as the most appropriate quantifiable variable for drawing tool life curve for micro-milling. The pattern of variation of ΔD_C matches with the typical tool life curve drawn earlier by Alauddin et al. (1995) [30] for macro-scale end milling process. The ΔD_C remains reasonably low within the abrasive and adhesive regimes; however, it increases steeply after chipping. Usually the tool rejection criteria are set based on the output product quality requirement. While the ΔD_C is established as the most appropriate variable in this article, the tool life for varying process parameters under different lubrication conditions will be reported in a subsequent communication after analysing the effect of progressive wear on machinability and feature surface and sub-surface quality [31].

7. Conclusion

This article demonstrates a methodology for precisely estimating the outer diameter reduction of a typical micro-milling tool during progressive tool wear analysis. Analytical formulas are framed for various wear scenarios and thereafter validated through minimum quantity lubrication (MQL) assisted sustainable micro-milling of Ti–6Al–4V using a 500 μm diameter TiAlN-coated two-flute tungsten carbide (WC/6Co) micro-mill. Based on the analysis of the results, following conclusions are drawn.

1. The fresh micro-mill, when engaged for machining, experiences rapid break-in wear for first 15 mm length of cut which is followed by gradual abrasion up to 85 mm cut. While edge radius increases with abrasion, the coating thickness also decreases leading to delamination and strong adhesion on the edge. First sign of edge-chipping is detected after 115 mm cut. Chipping again exposes fresh substate that further promotes adhesion. Further micro-milling using chipped tool results in repeated chipping and adhesion.
2. Edge radius (r_e) can be fairly measured during the abrasive and adhesive wear regimes. After chipping, the edge loses its rounded shape, and thus edge radius cannot be fairly measured. Instead, flank wear length (V_B) can be considered as the primary measurable and quantifiable parameter in the chipping wear regime.

3. Direct measurement of outer diameter by observing the micro-mill under a microscope is inherently associated with significant measurement error. Such data are also affected by inconsistency and negative wear rate that make them less reliable for further analysis. Thus direct measurement of diameter of the worn-out tool is discouraged.
4. It is feasible to precisely estimate the reduction in outer diameter owing to progressive tool wear using the geometry of the worn-out cutting edges. Relevant formulas with derivation for various wear scenarios (uniform abrasion, non-uniform abrasion, adhesion, and chipping wear) are presented here. Such estimated values of the outer diameter vary in a consistent manner with a positive wear rate. Thus estimated outer diameter values should be preferably used during progressive tool wear analysis.
5. Neither edge radius nor flank wear length is a suitable variable for drawing tool life curve in micro-milling. As the outer diameter reduction can be estimated across all regimes, it can be considered as the preferred index for drawing tool life curve. The estimated outer diameter of the 0.5 mm tool reduces by 4.4% at the end of 200 mm cut whereby two cutting edges suffer 33 μm and 38 μm flank flattening.

CRediT authorship contribution statement

Suman Saha: Problem definition, Methodology, Experimentation, Data curation, Formal analysis, Writing – original draft. **Sankha Deb:** Supervision, Resources. **Partha Pratim Bandyopadhyay:** Problem definition, Supervision, Writing – review & editing.

Declaration of competing interest

The authors declare that they have no known competing financial interests or personal relationships that could have appeared to influence the work reported in this paper.

Acknowledgment

This research did not receive any specific grant from funding agencies in the public, commercial, or not-for-profit sectors.

References

[1] J.C. Aurich, I.G. Reichenbach, G.M. Schüler, Manufacture and application of ultra-small micro end mills, CIRP Ann 61 (2012) 83–86, https://doi.org/10.1016/j.cirp.2012.03.012.
[2] M. Miranda, D. Serje, J. Pacheco, J. Bris, Tool edge radius wear and material removal rate performance charts for titanium micro-milling, Int. J. Precis. Eng. Manuf. 19 (2018) 79–84, https://doi.org/10.1007/s12541-018-0009-z.
[3] B.Z. Balázs, N. Geier, M. Takács, J.P. Davim, A review on micro-milling: recent advances and future trends, Int. J. Adv. Manuf. Technol. 112 (2020) 655–684, https://doi.org/10.1007/s00170-020-06445-w.
[4] L. Móricz, Z.J. Viharos, A. Németh, A. Szépligeti, M. Büki, Off-line geometrical and microscopic & on-line vibration based cutting tool wear analysis for micro-milling of ceramics, Measurement 163 (2020) 108025, https://doi.org/10.1016/j.measurement.2020.108025.
[5] İ. Ucun, K. Aslantas, F. Bedir, An experimental investigation of the effect of coating material on tool wear in micro milling of Inconel 718 super alloy, Wear 300 (2013) 8–19, https://doi.org/10.1016/j.wear.2013.01.103.
[6] A. Dadgari, D. Huo, D. Swailes, Investigation on tool wear and tool life prediction in micro-milling of Ti-6Al-4V, Nanotechnol. Precis. Eng. 1 (2018) 218–225, https://doi.org/10.1016/j.npe.2018.12.005.
[7] W. Khaliq, C. Zhang, M. Jamil, A.M. Khan, Tool wear, surface quality, and residual stresses analysis of micro-machined additive manufactured Ti–6Al–4V under dry and MQL conditions, Tribol. Int. 151 (2020) 106408, https://doi.org/10.1016/j.triboint.2020.106408.
[8] M. Sorgato, R. Bertolini, S. Bruschi, On the correlation between surface quality and tool wear in micro–milling of pure copper, J. Manuf. Process. 50 (2020) 547–560, https://doi.org/10.1016/j.jmapro.2020.01.015.
[9] C.S. Manso, S. Thom, E. Uhlmann, C.L. de Assis, E.G. del Conte, Tool wear modelling using micro tool diameter reduction for micro-end-milling of tool steel H13, Int. J. Adv. Manuf. Technol. 105 (2019) 2531–2542, https://doi.org/10.1007/s00170-019-04575-4.
[10] S. De Cristofaro, N. Funaro, G.C. Feriti, M. Rostagno, M. Comoglio, A. Merlo, et al., High-speed micro-milling: novel coatings for tool wear reduction, Int. J. Mach. Tool Manufact. 63 (2012) 16–20, https://doi.org/10.1016/j.ijmachtools.2012.07.005.
[11] L.L. Alhadeff, M.B. Marshall, D.T. Curtis, T. Slatter, Protocol for tool wear measurement in micro-milling, Wear 420–421 (2019) 54–67, https://doi.org/10.1016/j.wear.2018.11.018.
[12] X. Lu, Z. Jia, H. Wang, L. Si, Y. Liu, W. Wu, Tool wear appearance and failure mechanism of coated carbide tools in micro-milling of Inconel 718 super alloy, Ind. Lubric. Tribol. 68 (2016) 267–277, https://doi.org/10.1108/ILT-07-2015-0114.
[13] A.G. dos Santos, M.B. da Silva, M.J. Jackson, Tungsten carbide micro-tool wear when micro milling UNS S32205 duplex stainless steel, Wear 414–415 (2018) 109–117, https://doi.org/10.1016/j.wear.2018.08.007.
[14] V. Kumar, J. Mathew, Wear behavior of TiAlN coated WC tool during micro end milling of Ti-6Al-4V and analysis of surface roughness, Wear 424–425 (2019) 165–182, https://doi.org/10.1016/j.wear.2019.02.018.
[15] Y. Dai, K. Zhu, A machine vision system for micro-milling tool condition monitoring, Precis. Eng. 52 (2018) 183–191, https://doi.org/10.1016/j.precisioneng.2017.12.006.
[16] A. Varghese, V. Kulkarni, S.S. Joshi, Tool life stage prediction in micro-milling from force signal analysis using machine learning methods, ASME J. Manuf. Sci. Eng. 143 (2020), https://doi.org/10.1115/1.4048636.
[17] S.N. Oliaei, Y. Karpat, Influence of tool wear on machining forces and tool deflections during micro milling, Int. J. Adv. Manuf. Technol. 84 (2015) 1963–1980, https://doi.org/10.1007/s00170-015-7744-4.
[18] A.M. Abdelrahman Elkaseer, S.S. Dimov, K.B. Popov, R.M. Minev, Tool wear in micro-endmilling: material microstructure effects, modeling, and experimental validation, ASME J. Micro Nano-Manuf. 2 (2014), https://doi.org/10.1115/1.4028077.
[19] L.C. Silva, M.B. da Silva, Investigation of burr formation and tool wear in micromilling operation of duplex stainless steel, Precis. Eng. 60 (2019) 178–188, https://doi.org/10.1016/j.precisioneng.2019.08.006.
[20] A.S. Kumar, S. Deb, S. Paul, Tribological characteristics and micromilling performance of nanoparticle enhanced water based cutting fluids in minimum quantity lubrication, J. Manuf. Process. 56 (2020) 766–776, https://doi.org/10.1016/j.jmapro.2020.05.032.
[21] S. Saha, S. Deb, P.P. Bandyopadhyay, An analytical approach to assess the variation of lubricant supply to the cutting tool during MQL assisted high speed micromilling, J. Mater. Process. Technol. 285 (2020) 116783, https://doi.org/10.1016/j.jmatprotec.2020.116783.
[22] N. Shakoori, G. Fu, B. Le, J. Khaliq, L. Jiang, D. Huo, et al., An experimental investigation on tool wear behaviour of uncoated and coated micro-tools in micro-milling of graphene-reinforced polymer nanocomposites, Int. J. Adv. Manuf. Technol. 113 (2021) 2003–2015, https://doi.org/10.1007/s00170-021-06715-1.
[23] X. Liang, Z. Liu, B. Wang, Multi-pattern failure modes and wear mechanisms of WC-Co tools in dry turning Ti–6Al–4V, Ceram. Int. 46 (2020) 24512–24525, https://doi.org/10.1016/j.ceramint.2020.06.238.
[24] Y. Wang, B. Zou, C. Huang, Tool wear mechanisms and micro-channels quality in micro-machining of Ti-6Al-4V alloy using the Ti(C7N3)-based cermet micro-mills, Tribol. Int. 134 (2019) 60–76, https://doi.org/10.1016/j.triboint.2019.01.030.
[25] Y. Wang, B. Zou, J. Wang, Y. Wu, C. Huang, Effect of the progressive tool wear on surface topography and chip formation in micro-milling of Ti–6Al–4V using Ti(C7N3)-based cermet micro-mill, Tribol. Int. 141 (2020) 105900, https://doi.org/10.1016/j.triboint.2019.105900.
[26] S. Saha, S. Deb, P.P. Bandyopadhyay, Progressive wear based tool failure analysis during dry and MQL assisted sustainable micro-milling, Int. J. Mech. Sci. (2021) 106844, https://doi.org/10.1016/j.ijmecsci.2021.106844.
[27] M.A. Rahman, M. Rahman, M. Mia, M.K. Gupta, B. Sen, A. Ahmed, Investigation of the specific cutting energy and its effect in shearing dominant precision micro cutting, J. Mater. Process. Technol. 283 (2020) 116688, https://doi.org/10.1016/j.jmatprotec.2020.116688.
[28] V.A. Balogun, I.F. Edem, A.A. Adekunle, P.T. Mativenga, Specific energy based evaluation of machining efficiency, J. Clean. Prod. 116 (2016) 187–197, https://doi.org/10.1016/j.jclepro.2015.12.106.
[29] X. Zhang, T. Yu, J. Zhao, Surface generation modeling of micro milling process with stochastic tool wear, Precis. Eng. 61 (2020) 170–181, https://doi.org/10.1016/j.precisioneng.2019.10.015.
[30] M. Alauddin, M.A. El Baradie, M.S.J. Hashmi, Tool-life testing in the end milling of Inconel 718, J. Mater. Process. Technol. 55 (1995) 321–330, https://doi.org/10.1016/0924-0136(95)02035-7.
[31] R. Yadav, K. Vipindas, J. Mathew, Methodology for prediction of sub-surface residual stress in micro end milling of Ti-6Al-4V alloy, J. Manuf. Process. 62 (2021) 600–612, https://doi.org/10.1016/j.jmapro.2020.12.031.